Communication

Quantitative mapping of oxidative stress response to lithium cobalt oxide nanoparticles in single cells using multiplexed in situ gene expression analysis

Yi Cui, Eric S Melby, Arielle C Mensch, Elizabeth D. Laudadio, Mimi N Hung, Alice Dohnalkova, Dehong Hu, Robert J Hamers, and Galya Orr

Nano Lett., **Just Accepted Manuscript** • DOI: 10.1021/acs.nanolett.8b05172 • Publication Date (Web): 18 Feb 2019

Quantitative mapping of oxidative stress response to lithium cobalt oxide nanoparticles in single cells using multiplexed *in situ* gene expression analysis

Yi Cui,[1,3] Eric S. Melby,[1,4] Arielle C. Mensch,[1] Elizabeth D. Laudadio,[2] Mimi N. Hang,[2] Alice Dohnalkova[1], Dehong Hu[1], Robert J. Hamers,[2] Galya Orr[1,*]

1. Environmental Molecular Sciences Laboratory, Pacific Northwest National Laboratory, Richland, WA 99354

2. Department of Chemistry, University of Wisconsin, Madison, WI 53706

3. Present Address: MIT Media Lab, Cambridge, MA 02139

4. Present Address: Columbia Basin College, Pasco, WA 99301

* Corresponding Author: Galya Orr, Tel: 509-371-6127, Email: Galya.Orr@pnnl.gov

Abstract

Engineered nanoparticles (NPs) can negatively impact biological systems through induced generation of reactive oxygen species (ROS). Over-produced ROS cause biochemical damage and hence need to be effectively buffered by a sophisticated cellular oxidative stress response system. How this complex cellular system, which consists of multiple enzymes, responds to NP-induced ROS is largely unknown. Here we apply a single cell analysis to quantitatively evaluate 10 key ROS responsive genes simultaneously to understand how the cell prioritizes tasks and reallocates resources in response to NP-induced oxidative stress. We focus on rainbow trout gill epithelial cells – a model cell type for environmental exposure – and their response to the massive generation of ROS induced by lithium cobalt oxide (LCO) NPs, which are extensively used as cathode materials in lithium ion batteries. Using multiplexed fluctuation localization imaging-based fluorescence *in situ* hybridization (fliFISH) in single cells, we found a shift in the expression of oxidative stress response genes with initial increase in genes targeting superoxide species, followed by increase in genes targeting peroxide and hydroxyl species. In contrast, Li^{+} and Co^{2+}, at concentrations expected to be shed from the NPs, did not induce ROS generation but showed a potent inhibition of transcription for all 10 stress response genes. Taken together, our findings suggest a "two-hit" model for LCO NP toxicity, where the intact LCO NPs induce high levels of ROS that elicit sequential engagement of stress response genes, while the released metal ions suppress the expression of these genes. Consequently, these effects synergistically drive the exposed cells to become more vulnerable to ROS stress and damage.

Key words: single molecule FISH, super resolution fluorescence imaging**,** gene expression, reactive oxygen species, metal oxide nanoparticles, toxicity

Intercalated lithium compounds constitute one of the most widely used materials in rechargeable battery cells. Among cathode materials for lithium-ion batteries, lithium cobalt oxide (LCO) features high energy density and stable capacity, thus is extensively implemented in portable electronics.[1, 2] Producing LCO at the nanoscale enhances electron transport and therefore improves the battery performance.[3, 4] However, the exponential growth of the lithium-ion battery industry imposes risks to our environment and ecological systems considering the fact that our infrastructure for battery recycling is underdeveloped.[5] A growing body of evidence has suggested that LCO and related NPs induce stress and toxicity in various model systems,[6-10] though the underlying mechanism is still unclear. During electrochemical cycling, LCO NPs can be fractured into sub-100 nm "nano-flakes".[11] When disposed in the environment, the sheet-like LCO NPs (**Figure S1**) could negatively impact living organisms and cells. A direct outcome of exposure to many types of engineered NPs is excessive generation of reactive oxygen species (ROS) and their subsequent adverse effects.[12-15] Industrial manufacturers have attempted to reduce the environmental impact of lithium-ion batteries, such as using thin coatings to prevent dissolution of transition metal ions from the cathode.[16] However, we and others have shown that the intact LCO NP is responsible for ROS generation and adverse cellular effects.[8, 10] Therefore, molecular level understanding of these processes should be a prerequisite for developing effective strategies for mitigating adverse effect and environmentally sustainable disposal of these NPs.

ROS are naturally generated in living organisms and play fundamental roles when maintained within physiological ranges. However, upon exposure to certain metal ions or nanomaterials, living cells often show excessive ROS generation and reactivate relevant antioxidant responses.[17, 18] According to the step-wise chemical reactions in biological systems, ROS can be categorized into two main groups: primary ROS and secondary ROS.[19] Primary ROS refers to superoxide anion ($O_2^{-\bullet}$) produced from oxygen activation, while secondary ROS arise after primary ROS oxidize other molecules such as H_2O to become radicals. The delicate balance between ROS generation and elimination is maintained by an intricate network comprising enzymatic and non-enzymatic factors.[18] Antioxidant enzymes provide cells with necessary protection against ROS stress and dynamically respond to the stress level through regulated gene expression. While our previous study has shown that LCO NPs induce massive ROS generation,[10] the relationships between LCO NP exposure and the fine balance that the cell maintains in the expression of antioxidant genes has been largely unknown.

Conventional methods for gene expression analysis, such as PCR and RNA-seq, often use a large number of cells or bulk samples, which therefore only reflect the population-based change trend. However, it has been shown that transcription is highly dynamic, and substantial heterogeneity in the RNA transcript numbers, even for the same gene could exist at the single-cell level.[20, 21] Hence, high-throughput single-cell studies pave the way for our better understanding of biological functions and regulations.[22, 23] For cells exposed to nanomaterials, the uptake efficiency and molecular response greatly vary, leading to differential gene expression and survival outcomes.[24] Studying NP-inducted alterations in transcription and subsequently toxicity at the single-cell resolution will enable a refined characterization of the interplay among the molecular processes and facilitate the development of preventative approaches.

Fluorescence *in situ* hybridization (FISH) is a direct, imaging-based tool for localization and quantification of nucleic acids in single cells.[25-27] Recently, we have developed an improved FISH technique, called fluctuation localization imaging-based FISH (fliFISH) for accurate counting of RNA molecules in single cells with nanometer resolution.[28] fliFISH takes advantage of photoswitchable dyes and super-resolution localization microscopy to enhance the detection specificity and localization precision, while supporting the use of a small number of FISH probes. fliFISH has been demonstrated to be compatible with a broad range of fluorophores and thus holds the potential for combinatorial fluorescence barcoding and multiplexing applications. In this study, we used multiplexed fliFISH to target a panel of 10 key ROS stress response genes in rainbow trout gill epithelial cells, a model cell type for environmental exposure, following exposures to LCO NPs and their shed ions. We identified a sequence of molecular events that shed light on the cellular response to the massive generation of ROS by LCO NPs and their subsequent toxicity.

Accurate quantification of transcripts for multiple genes in a single cell using multiplexed fliFISH: fliFISH utilizes photoswitchable dyes to distinguish between true and false hybridization signals. Upon introducing a set of predesigned oligonucleotide probes, each tagged with a predetermined number of fluorophores and complementary to a sub-area on the target RNA molecule, a known number of fluorophores is expected to exist in a diffraction-limited area (**Figure 1A**). Knowing the average on-time fraction for a single fluorophore/probe, the ensemble on-time fraction of the probe set at a correctly hybridized position can be predicted and identified with a proper threshold. In general, three major noise sources would occur in a typical FISH

experiment: autofluorescence, non-specific binding of stray probes, and aggregated probes. Distinguishing the signals of these sources of noise from true signals, coming from correctly hybridized probes, is very challenging for most intensity-based localization algorithms, which rely on one-shot imaging. This is especially difficult when using a limited number of probes for each transcript. In comparison, fliFISH enables efficient identification and distinguishing between the noise and true signals based on their distinct photoblinking patterns in the time domain (**Figure 1B-E**). In principle, within a specified time window, correctly bound FISH probes give a loci-dependent predictable number of emission events (**Figure 1B**). In contrast, autofluorescence give no photoswitchable emissions (**Figure 1C**), aggregated probes give rise to clustered emissions (*i.e.,* too many events) (**Figure 1D**), and stray or nonspecifically bound probes give rise to sparse emissions (*i.e.,* too few events) (**Figure 1E).** Only at the true hybridization location a predetermined number of events can be detected (**Figure 1B**). In addition, during the fliFISH image processing, the centroid of each emission event is precisely localized, resulting in super-resolution capacity of the method, which also adds to its high accuracy. For example, multiple transcripts for highly expressed genes can be resolved and counted in a diffraction-limited spot.

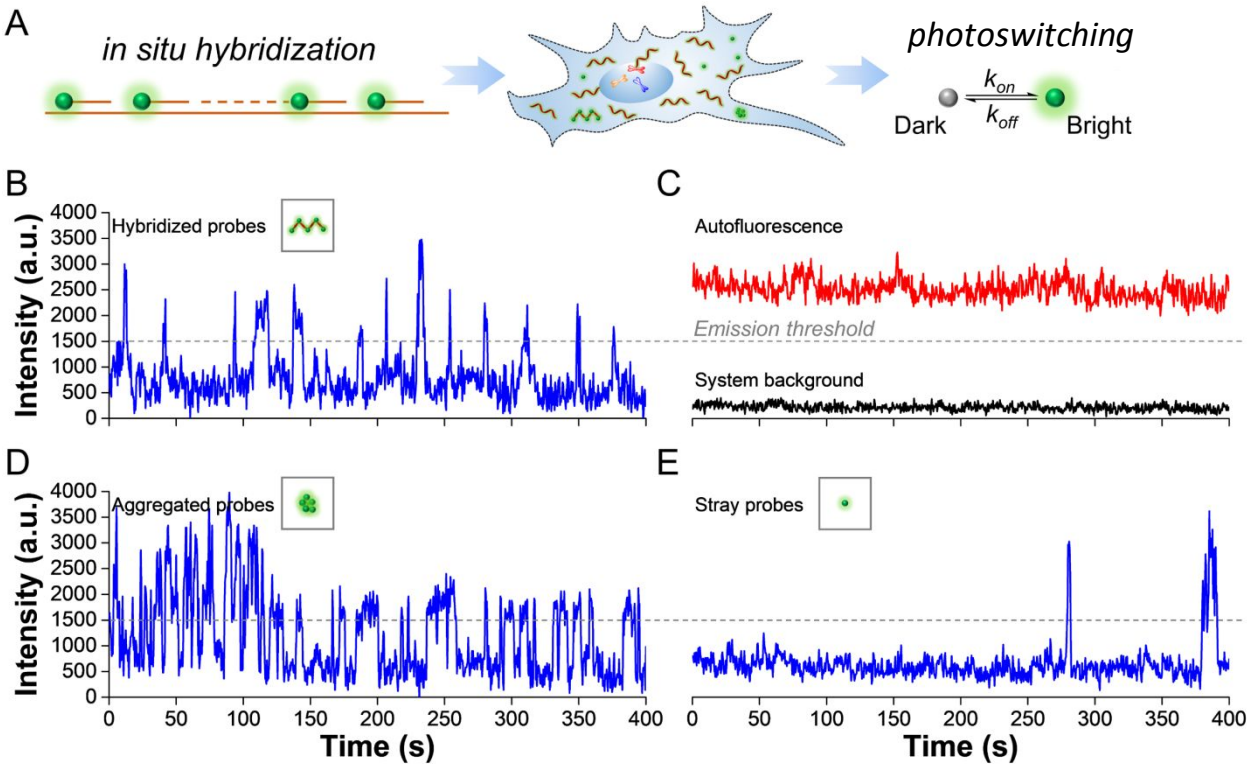

Figure 1. The fliFISH concept and mechanism. (A) fliFISH utilizes multiple oligonucleotide probes, each tagged with a photoswitchable dye, to target a transcript of a given gene. The use of

photoswitchable dyes enables the identification of different fluorescence blinking patterns. (B) A predetermined number of photoblinking events can be detected only from correctly hybridized loci. In contrast, autofluorescence shows no blinking events (C), while aggregated probes give rise to excessive number of events (D), and nonspecifically bound stray probes show sparse events (E).

By utilizing photoswitchable dyes with different emission spectra, multiplexed fliFISH can be implemented to target transcripts of multiple genes in a given cell. Barcoding RNA targets with more than one color can greatly expand the throughput. For instance, assigning two colors to each target gene from five available colors, 10 genes can be simultaneously analyzed at the single-cell level: doubling the throughput over the single-color strategy. In two-color barcoding, an RNA transcript is recognized only when it is detected under both assigned channels (**Figure 2A**). Moreover, this spectral barcoding does not require an extended acquisition time, but substantially improves the detection throughput and specificity. After imaging and processing data from all five channels, the transcripts of 10 genes can be quantified and localized in single cells (**Figure 2B**).

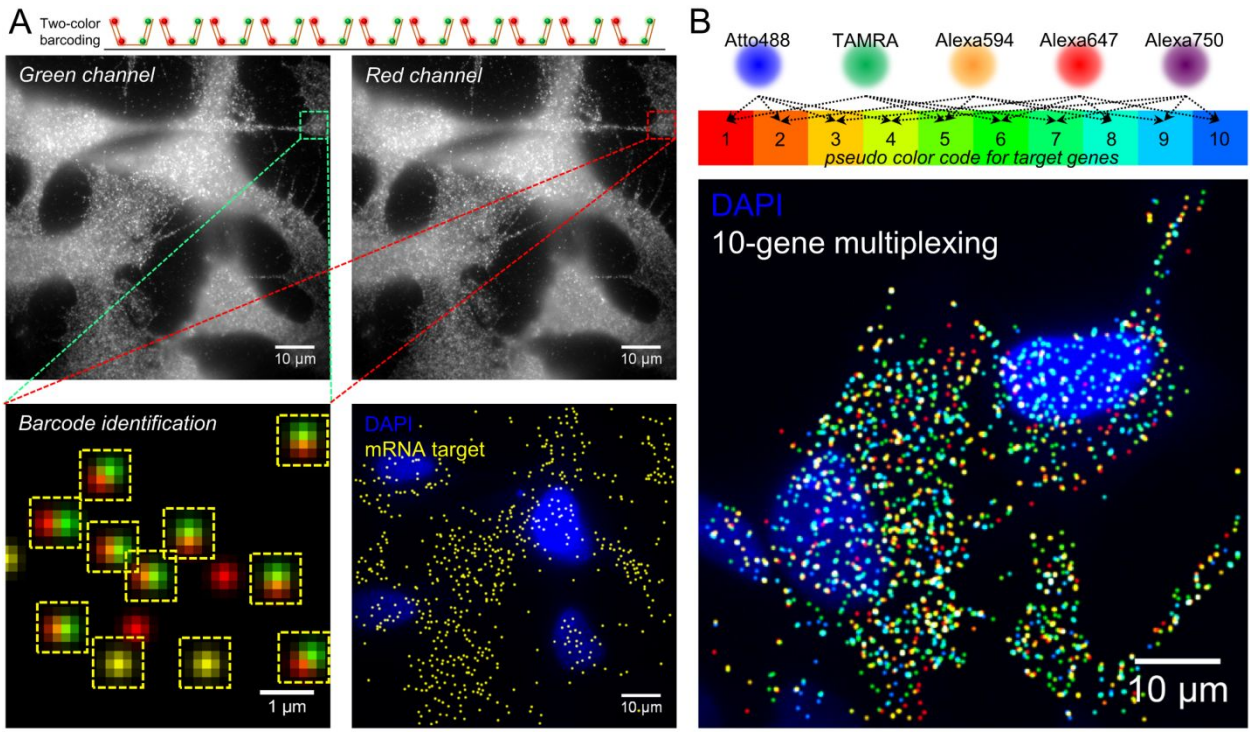

Figure 2. Demonstration of barcoded gene detection with multiplexed fliFISH in single cells. (A) A two-color barcode is assigned to each gene, where the targeted mRNA transcript should be detected under both color channels only at successfully hybridized positions. (B) Using 5 available dyes, 10 antioxidant genes are barcoded in rainbow trout gill epithelial cells. After imaging and

processing all 5 color channels, the quantity and position of transcripts for each of the 10 genes can be precisely determined.

Assigning fluorescence barcodes and categories to oxidative stress response genes: As mentioned above, ROS in a biological system can be categorized into two major groups: primary ROS and secondary ROS, based on their sequential order of generation (**Figure 3A**). The demonstrated induction of ROS generation in response to metal oxide NP exposures could reflect the over production of $O_2^{-\bullet}$, •OH and H_2O_2 that are highly reactive with biomolecules.[17] Non-enzymatic antioxidants, including vitamin C, E, glutathione and carotenoids, provide fast but limited protection against ROS-induced biological damages. A more flexible and sustainable response to ROS stress requires long-term involvement of enzymatic factors. Here, we categorize the ROS stress response genes to three functional groups according to their different reactive substances (**Figure 3A**). We define the enzymes that are responsible for removal or detoxification of primary ROS and metal ions as the primary defense. For example, superoxide dismutase (SOD) is one of the most effective enzymatic antioxidant catalyzing the conversion of $O_2^{-\bullet}$ to the less reactive H_2O_2 in cells: $2O_2^{\bullet-} + 2H^+ \xrightarrow{SOD} H_2O_2 + O_2$.[29] We define the enzymes that react with secondary ROS as secondary defense. For example, catalase (CAT) is a conserved enzyme across species that promotes the removal of H_2O_2 in peroxisomes: $2H_2O_2 \xrightarrow{CAT} 2H_2O + O_2$.[30] Glutathione peroxidase (GPx), glutathione-S-transferase (GST) and thioredoxin (TRX) are also essential enzymes that help reduce H_2O_2, organic peroxide and oxidized proteins in secondary defense. Some antioxidant enzymes in the primary and secondary defense systems are oxidized after reaction with ROS but can be reduced back to the original functional state. Hence, we define these enzymes, which enable the recycling of oxidized antioxidants, as the defense recovery system, including GPx reductase (GR), TRX reductase (TR) and other relevant factors.

In this study, we chose *Oncorhynchus mykiss* (rainbow trout) gill epithelial cells as a model system. These cells are targets for NP exposure in the aquatic environment, potentially also due to disposed battery wastes. Our previous research has demonstrated the uptake of LCO NPs and ROS-related cytotoxicity in this cell line.[10] We selected 10 key genes that represent the three main functional groups in the oxidative stress response system (primary defense, secondary defense and defense recovery). The sequences for the 10 genes in the rainbow trout genome were retrieved from the NCBI genome database (NCBI *Oncorhynchus mykiss* Annotation Release 100). Fifteen unique

sequences (20 nucleotide-long each) were identified for each gene (**Table S2**) and were used to reconstruct the fliFISH probes as described under Supporting Information. Each gene target was assigned a two-color barcode (**Figure 3B**). In **Figure 3B**, genes that belong to the primary defense category are highlighted in red, genes that belong to the secondary defense category are highlighted in green, and genes that belong to the defense recovery category are highlighted in blue. Based on this strategy, not only can the transcript number of these ten genes be precisely counted, but the expression ratio between each gene category can be quantified (**Figure 3C**).

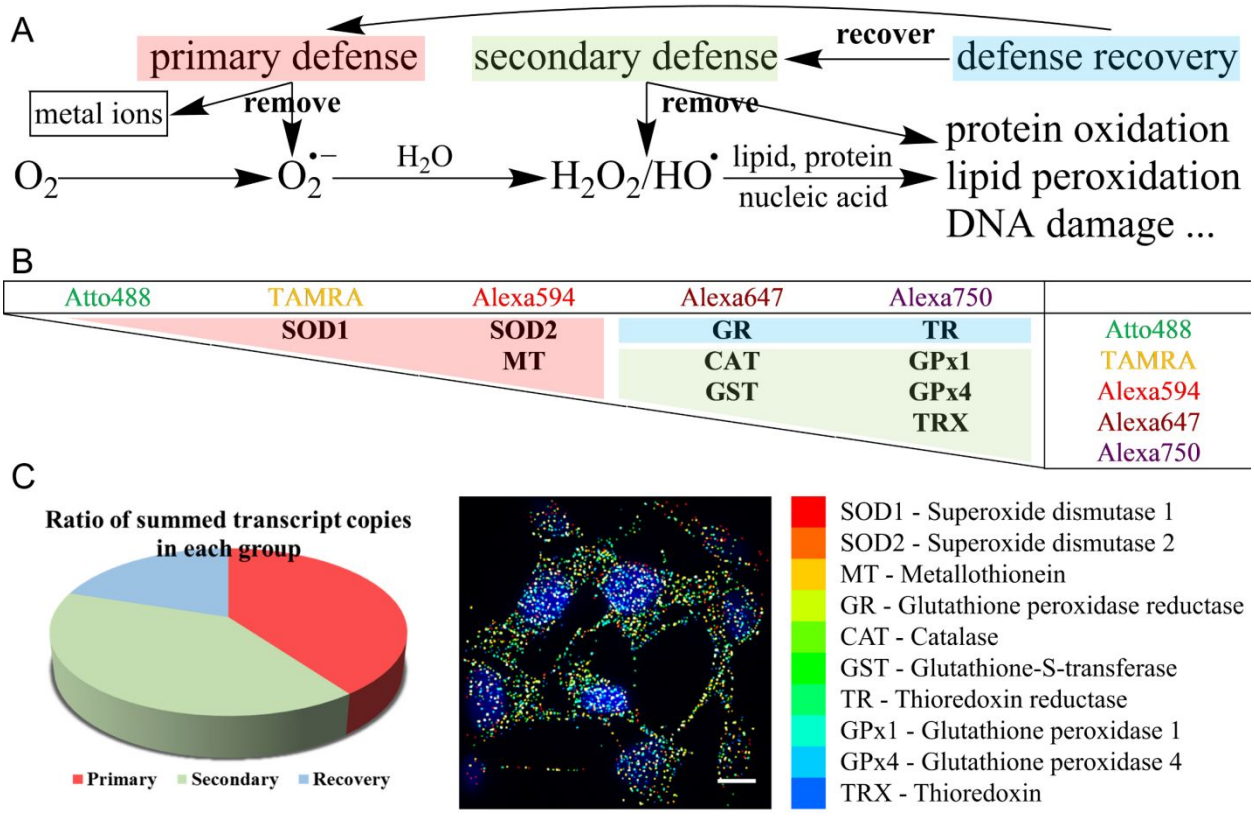

Figure 3. Quantitative gene expression analysis of 10 oxidative stress response genes in single rainbow trout gill epithelial cells using multiplexed fliFISH. (A) Oxidative stress response enzymes can be categorized into three functional groups: primary defense, secondary defense, and defense recovery based on their different reactive substrates. (B) 10 representative ROS stress response genes were selected and assigned a two-color barcode for fliFISH. Genes belonging to the primary defense are highlighted in red, those belonging to the secondary defense are highlighted in green, and those belonging to the recovery defense are highlighted in blue. (C) Downstream analysis includes calculating ratios of summed transcript copies in each of the three

stress response groups for each cell, as well as averaged values for all the cells, as demonstrated in the pie chart for unexposed cells (primary : secondary : recovery = 40% : 40% : 20%). For visualization, each gene was assigned with a pseudo color, as demonstrated in the fliFISH image.

Mapping oxidative stress responses to LCO NPs and their shed ions in single cells: Using multiplexed fliFISH, we studied the expression levels of key ROS stress response genes in cells exposed to LCO NPs at 100 μg/mL, as well as to lithium and cobalt ions at 100 μM, which are expected to be shed from the NPs at the exposure concentration used here.[10] First, all 10 selected genes experienced significant down-regulation (>2-fold) in cells exposed to lithium or cobalt ions for 24 hours, as well as in cells grown in low-nutrient media (Hanks' balanced salt solution) for 12 hours (**Table 1**). **Figures 4A and S2A** present this down regulation across all treatments by plotting the summed transcript counts for the genes under each of the three oxidative stress response groups for individual cells, represented by single dots. We then calculated the percent of transcript copies in each of the three stress response groups for each cell (**Figures 4B and S2B**). Interestingly, we found that the transcript ratios between the three groups did not change in cells exposed to lithium ions or grown in low-nutrient medium compared to unexposed cells. The ratio of the average transcript counts under these exposure conditions was 40% : 40% : 20% for the primary, secondary, and recovery groups, respectively. However, in cells exposed to the cobalt ions the primary defense and recovery genes showed down-regulation to a greater extent than the secondary genes, and therefor a slight increase in the percent of transcript counts for genes under the secondary defense group (primary : secondary : recovery = 31% : 49% : 20%) (**Figures 4B, S2B and S4A**). These results are in agreement with reports showing that lithium and cobalt ions could inhibit the expression of antioxidant genes, but the underlying mechanism remains largely unknown.[31, 32] Likewise, nutrient deprivation leads to a global suppression of gene expression.[33] The advantage of our multiplexing single cell analysis is the ability to simultaneously target key genes in a molecular network to decipher how a single cell prioritizes tasks and reallocates resources under stress conditions. Herein, the change in the level of suppression ratio by cobalt ions could imply that these ions induce secondary ROS generation to a higher level than the level induced by lithium ions, and in response, the cells maintain the expression of secondary defense genes at a relatively higher level to ensure survival.

Intriguingly, when the cells were exposed to LCO NPs, no unidirectional change in transcription was observed for the 10 genes (**Table 1**, **Figure S5**), while the ratio between the three groups of oxidative stress response genes experienced changes over time (**Figures 4C and S3A**). After 24 h of exposure to 100 μg/mL LCO NPs, the proportion of the primary defense group increased compared to the proportion in the unexposed cells (primary : secondary : recovery = 52% : 33% : 15%), with SOD1 as the most significantly up-regulated gene (**Table 1**; **Figures S4B and S5**). In contrast, after 48 h of exposure, the proportion of the secondary defense group showed up-regulation (primary : secondary : recovery = 33% : 47% : 20%), with CAT as the most significantly up-regulated gene (**Table 1, Figures 4D, S3B, S4B and S5**). As a positive control for oxidative stress, the cells were exposed to 100 μM H_2O_2 for over 24 h. H_2O_2 is a prevalent secondary ROS and indeed, such exposure significantly up-regulated the expression and proportion of secondary defense genes (primary : secondary : recovery = 33% : 48% : 19%) (**Figures 4D and S4B**). Taken together, our results suggest that the composition of antioxidant gene pool continuously adapts when exposed to LCO NPs, which is also consistent with the sequential generation of different ROS. During the early exposure, cells enhance the expression of primary defense genes to resist primary ROS. Over time, primary ROS are gradually converted to secondary ROS in the cells and in response, more cellular resources are used to express secondary defense genes.

Condition / Gene	Unexposed	100 μM Li^+ (24h)	100 μM Co^{2+} (24h)	Low nutrition (12h)	100 μg/mL LCO NPs (24h)	100 μg/mL LCO NPs (48h)	100 μM H_2O_2 (24-48h)
SOD1	93.4±34.8	40.2±16.6	40.1±17.7	28.7±16.3	135.1±41.5	91.6±29.8	117.2±38.0
SOD2	70.6±26.1	25.5±10.5	26.6±9.2	20.5±11.8	98.0±28.1	55.3±18.4	89.2±23.3
MT	72.9±28.6	29.5±16.1	39.8±12.0	19.8±12.4	96.4±30.4	54.2±19.2	97.2±28.3
CAT	57.7±35.9	27.3±15.9	44.0±11.5	14.3±9.5	66.0±27.0	73.8±22.5	99.2±31.1
GST	48.3±24.2	21.0±14.0	34.1±12.9	13.1±10.2	52.4±23.0	51.1±14.9	83.8±17.5
GPx1	51.9±27.2	23.9±11.6	33.1±14.7	14.8±10.0	36.2±15.7	62.9±17.3	87.9±27.4
GPx4	43.1±24.2	19.8±8.6	22.3±7.4	13.2±8.4	30.6±12.9	41.7±11.7	78.7±10.9
TRX	51.6±26.2	14.6±8.0	32.4±10.2	12.2±8.0	31.5±11.5	52.8±12.7	84.1±20.4
TR	57.5±22.6	20.5±11.0	28.3±13.0	14.6±9.7	39.8±13.4	55.9±15.9	83.6±17.5
GR	59.8±21.5	17.8±12.0	35.3±12.6	13.1±8.1	63.0±25.1	68.5±21.3	95.0±26.2

Table 1. Averaged transcript copy number for the 10 ROS responsive genes in single cells under the different exposure conditions. (Mean ± SD, n = 30-50 cells per condition)

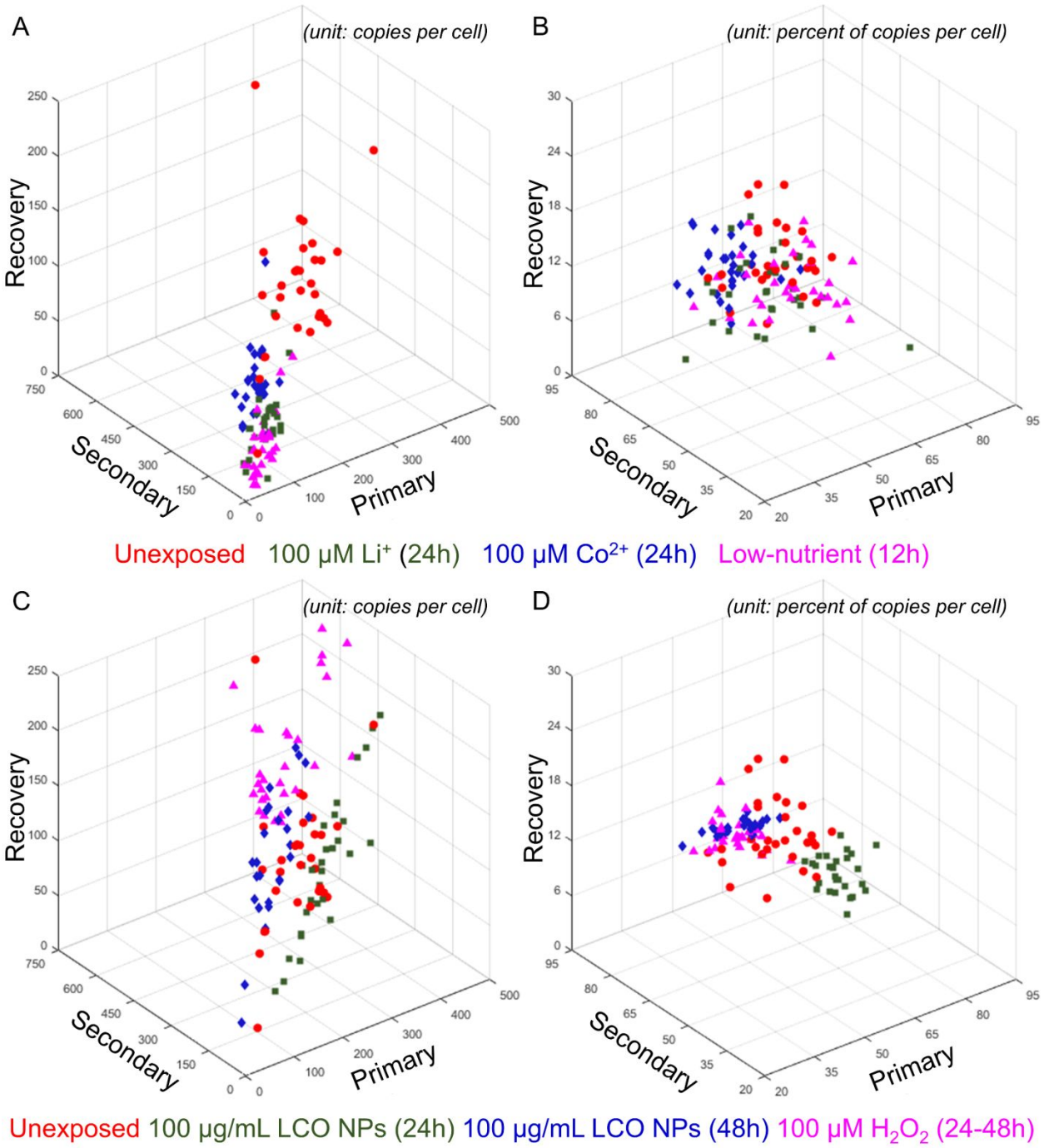

Figure 4. The transcript copy numbers and ratios of the three oxidative stress response groups in cells exposed to LCO NPs and their expected shed ions. (A) The transcript counts in each of the three stress response groups and (B) the transcript count ratios between the three groups for each cell (dot) exposed to lithium ions (green) or cobalt ions (blue) for 24 h, or grown in low-nutrient medium (magenta) for 12 h. (C) The transcript counts and (D) ratios of the three stress response

groups in single cells (dots) exposed to LCO NPs or H_2O_2 for 24 h and 48 h. Each dot in the graphs represents measurements for a single cell (total of 30-50 cells per treatment).

The time-dependent ROS generation and heterogeneous cellular responses prompted us to develop an approach for direct visualization of the antioxidant state at a single-cell resolution. We chose to reconstruct the gene expression information into color-coded maps by assigning the ratio of the three oxidative stress response groups in each cell with respective RGB values as shown in **Figure 5A**. For instance, if the transcript numbers of primary defense, secondary defense and defense recovery in a cell are 400, 400 and 200, respectively, the assigned values in the red, green and blue domains could be 0.4, 0.4 and 0.2, respectively. The mixed color will then appear as "brown" in the reconstructed image. This approach allows us to visualize the shift in the composition of the three oxidative stress response groups in cells exposed to LCO NPs over time. **Figure 5B** demonstrates the single cell increase in the transcription of the primary defense group (red) at 24 hours, and the increase in the transcription of the secondary defense group (green) at 48 hours.

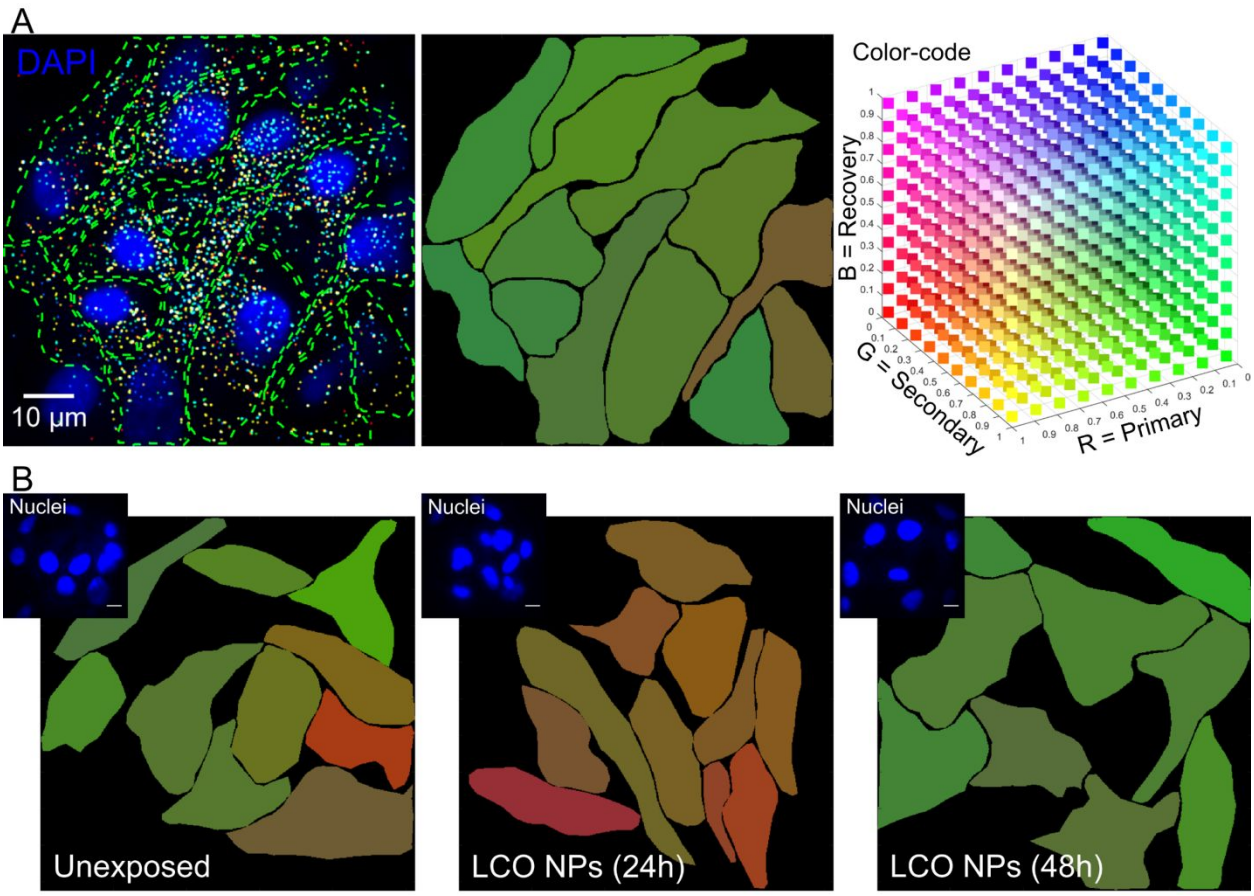

Figure 5. Visualizing the composition of the three oxidative stress response groups in single cells using reconstructed red, green and blue color-map images. (A) Right: proportional to the measured copy numbers, a particular weight value of red color ("R" element) is assigned to the primary defense group; weight value of green color ("G" element) is assigned to the secondary defense group; and weight value of blue color ("B" element) is assigned to the defense recovery group. Middle: The RGB image is then reconstructed by mixing these three values, where the changes in the ratio between the three stress response groups can be detected by the change in the mixed color assigned to each cell. Left: The cell nucleus is stained with DAPI (blue) and the cell boundary is shown with the dashed line, determined based on the bright-field image. Each dot represents a transcript copy for each of the 10 genes, differentiated by pseudo-colors as listed in Figure 3C. (B) Reconstructed RGB images demonstrating the shift in the ratio between the three oxidative stress response groups. A shift to the red color (primary defense genes) is detected in cells exposed to LCO NPs for 24 h (middle image), whereas a shift to the green color (secondary defense genes) is detected in cells exposed to LCO NPs for 48 h (left image).

A "two-hit" model can explain LCO NP-induced ROS stress and toxicity: Previously, we reported the internalization and accumulation of LCO NPs in gill epithelial cells by transmission electron microscopy (TEM).[10] We also showed that the LCO NPs, unlike lithium or cobalt ions, induced strong ROS generation and other cytotoxic effects. These results indicate that the intact LCO NP is the primary cause for ROS generation and stress. Here, we measured ROS generation over longer time periods, from 2 h to 48 h, using a fluorescent sensor (**Figure S6A**). Cells exposed to 100 μg/mL LCO NPs for 2 h showed strong fluorescence signals, indicating high levels of ROS generation. A gradual reduction in the signal intensity was observed over 48 h, suggesting the activation of the intracellular antioxidant stress response system. In contrast, cells exposed to 100-500 μM lithium or cobalt ions for 24 h (the equivalent concentration range for ions released from LCO NPs in the culture medium) showed subtle increase in fluorescence signals, confirming that the ions are not the main ROS inducer (**Figure S6B**). Combining these findings with our gene expression analysis, a "two-hit" model for the LCO NP-induced ROS stress and toxicity is proposed (**Figure S6C**). The first "hit" originates from the internalized LCO NPs that are strong ROS inducers due, in part, to their high surface area and reactivity. Along with excessive ROS generation, lithium and cobalt ions are gradually released from the NPs. These ions, in turn, suppress the activation and expression of ROS stress response genes, which strike the second "hit"

to the exposed cells. This model could explain why certain complex metal oxide NPs bring about high levels of toxicity compared with the composition of their elements. Ultimately, this study points to the potential harmful effect of lithium-ion batteries containing LCO-NPs on the environment and the need to carefully control their disposal.

Table of Content Figure

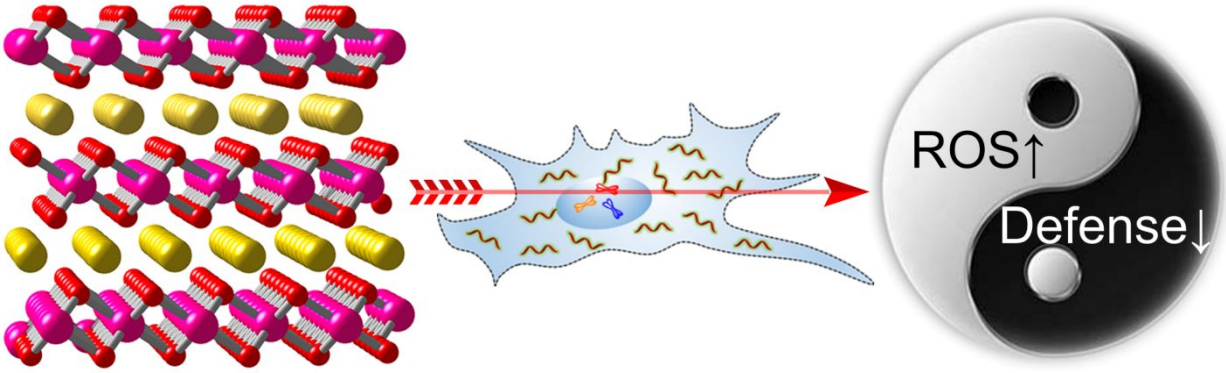

Acknowledgement

This work was supported by the National Science Foundation under the Center for Sustainable Nanotechnology, CHE-1503408. The CSN is part of the Centers for Chemical Innovation Program. Development of the multiplexed *in situ* gene expression analysis was supported in part by the Microbiome in Transition Initiative at Pacific Northwest National Laboratory (PNNL). This research used instrumentations at the Environmental Molecular Sciences Laboratory (EMSL), a DOE Office of Science User Facility sponsored by the Office of Biological and Environmental Research and located at PNNL.

Supporting Information

The Supporting Information is available free of charge on the ACS Publications website at DOI:

….

Expanded materials and methods and supporting figures, including additional details about the experimental methods, nanoparticle characterization, 2D presentations of single cell transcript copy number and percent, bar graph presentations of averaged transcript copy number and percent, intracellular ROS detection and quantification using fluorescent probe (PDF)

References

1. Whittingham, M. S. *Chem. Rev.* **2004,** 104, (10), 4271-301.
2. Nitta, N.; Wu, F. X.; Lee, J. T.; Yushin, G. *Mater. Today* **2015,** 18, (5), 252-264.
3. Poizot, P.; Laruelle, S.; Grugeon, S.; Dupont, L.; Tarascon, J. M. *Nature* **2000,** 407, (6803), 496-9.
4. Bruce, P. G.; Scrosati, B.; Tarascon, J. M. *Angew. Chem. Int. Ed. Engl.* **2008,** 47, (16), 2930-46.
5. Dunn, J. B.; Gaines, L.; Kelly, J. C.; James, C.; Gallagher, K. G. *Energy Environ. Sci.* **2015,** 8, (1), 158-168.
6. Dogangun, M.; Hang, M. N.; Troiano, J. M.; McGeachy, A. C.; Melby, E. S.; Pedersen, J. A.; Hamers, R. J.; Geiger, F. M. *ACS Nano* **2015,** 9, (9), 8755-65.
7. Hang, M. N.; Gunsolus, I. L.; Wayland, H.; Melby, E. S.; Mensch, A. C.; Hurley, K. R.; Pedersen, J. A.; Haynes, C. L.; Hamers, R. J. *Chem. Mater.* **2016,** 28, (4), 1092-1100.
8. Bozich, J.; Hang, M.; Hamers, R.; Klaper, R. *Environ. Toxicol. Chem.* **2017,** 36, (9), 2493-2502.
9. Gunsolus, I. L.; Hang, M. N.; Hudson-Smith, N. V.; Buchman, J. T.; Bennett, J. W.; Conroy, D.; Mason, S. E.; Hamers, R. J.; Haynes, C. L. *Environmental Science-Nano* **2017,** 4, (3), 636-646.
10. Melby, E. S.; Cui, Y.; Borgatta, J.; Mensch, A. C.; Hang, M. N.; Chrisler, W. B.; Dohnalkova, A.; Van Gilder, J. M.; Alvarez, C. M.; Smith, J. N.; Hamers, R. J.; Orr, G. *Nanotoxicology* **2018**, 1-16. doi: 10.1080/17435390.2018.1508785.
11. Wang, H. F.; Jang, Y. I.; Huang, B. Y.; Sadoway, D. R.; Chiang, Y. T. *J. Electrochem. Soc.* **1999,** 146, (2), 473-480.
12. Nel, A.; Xia, T.; Madler, L.; Li, N. *Science* **2006,** 311, (5761), 622-7.
13. Huang, C. C.; Aronstam, R. S.; Chen, D. R.; Huang, Y. W. *Toxicol. In Vitro* **2010,** 24, (1), 45-55.
14. Dominguez, G. A.; Lohse, S. E.; Torelli, M. D.; Murphy, C. J.; Hamers, R. J.; Orr, G.; Klaper, R. D. *Aquat. Toxicol.* **2015,** 162, 1-9.
15. Choudhury, S. R.; Ordaz, J.; Lo, C. L.; Damayanti, N. P.; Zhou, F.; Irudayaraj, J. *Toxicol. Sci.* **2017,** 156, (1), 261-274.
16. Suresh, A. K.; Pelletier, D. A.; Doktycz, M. J. *Nanoscale* **2013,** 5, (2), 463-74.

17. Valko, M.; Rhodes, C. J.; Moncol, J.; Izakovic, M.; Mazur, M. *Chem. Biol. Interact.* **2006,** 160, (1), 1-40.

18. Birben, E.; Sahiner, U. M.; Sackesen, C.; Erzurum, S.; Kalayci, O. *World Allergy Organ J* **2012,** 5, (1), 9-19.

19. Zorov, D. B.; Juhaszova, M.; Sollott, S. J. *Physiol. Rev.* **2014,** 94, (3), 909-50.

20. Golding, I.; Paulsson, J.; Zawilski, S. M.; Cox, E. C. *Cell* **2005,** 123, (6), 1025-36.

21. Raj, A.; Peskin, C. S.; Tranchina, D.; Vargas, D. Y.; Tyagi, S. *PLoS Biol.* **2006,** 4, (10), e309.

22. Crosetto, N.; Bienko, M.; van Oudenaarden, A. *Nat. Rev. Genet.* **2015,** 16, (1), 57-66.

23. Yuan, G. C.; Cai, L.; Elowitz, M.; Enver, T.; Fan, G.; Guo, G.; Irizarry, R.; Kharchenko, P.; Kim, J.; Orkin, S.; Quackenbush, J.; Saadatpour, A.; Schroeder, T.; Shivdasani, R.; Tirosh, I. *Genome Biol.* **2017,** 18, (1), 84.

24. Mitchell, H. D.; Markillie, L. M.; Chrisler, W. B.; Gaffrey, M. J.; Hu, D.; Szymanski, C. J.; Xie, Y.; Melby, E. S.; Dohnalkova, A.; Taylor, R. C.; Grate, E. K.; Cooley, S. K.; McDermott, J. E.; Heredia-Langner, A.; Orr, G. *ACS Nano* **2016,** 10, (11), 10173-10185.

25. Levsky, J. M.; Shenoy, S. M.; Pezo, R. C.; Singer, R. H. *Science* **2002,** 297, (5582), 836-40.

26. Raj, A.; van den Bogaard, P.; Rifkin, S. A.; van Oudenaarden, A.; Tyagi, S. *Nat. Methods* **2008,** 5, (10), 877-9.

27. Cui, Y.; Liu, J.; Irudayaraj, J. *Wiley Interdiscip Rev Nanomed Nanobiotechnol* **2017,** 9, (4).

28. Cui, Y.; Hu, D.; Markillie, L. M.; Chrisler, W. B.; Gaffrey, M. J.; Ansong, C.; Sussel, L.; Orr, G. *Nucleic Acids Res.* **2018,** 46, (2), e7.

29. McCord, J. M.; Fridovich, I. *J. Biol. Chem.* **1969,** 244, (22), 6049-55.

30. Gaetani, G. F.; Ferraris, A. M.; Rolfo, M.; Mangerini, R.; Arena, S.; Kirkman, H. N. *Blood* **1996,** 87, (4), 1595-1599.

31. Allagui, M. S.; Vincent, C.; El feki, A.; Gaubin, Y.; Croute, F. *Biochim. Biophys. Acta* **2007,** 1773, (7), 1107-15.

32. Tkaczyk, C.; Huk, O. L.; Mwale, F.; Antoniou, J.; Zukor, D. J.; Petit, A.; Tabrizian, M. *J. Biomed. Mater. Res. A* **2010,** 94, (2), 419-25.

33. Gameiro, P. A.; Struhl, K. *Cell Rep* **2018,** 24, (6), 1415-1424.